

# Knowledge Enhanced Conditional Imputation for Healthcare Time-series

Linglong Qian<sup>1\*</sup>, Zina Ibrahim<sup>1\*</sup>, Hugh Logan Ellis<sup>1,6</sup>, Ao Zhang<sup>5</sup>,  
Yuezhou Zhang<sup>1</sup>, Tao Wang<sup>1</sup>, Richard JB Dobson<sup>1,2</sup>

<sup>1\*</sup>Department of Biostatistics and Health Informatics, King's College  
London, London, UK.

<sup>2</sup>South London and Maudsley NHS Foundation Trust, United Kingdom.

<sup>3</sup>University College London, London, UK.

<sup>4</sup>Health Data Research UK, University College London, London, UK.

<sup>5</sup>Wellcome Centre for Human Genetics, Nuffield Department of  
Medicine, University of Oxford, Oxford, UK.

<sup>6</sup>Department of Medicine, King's College Hospital NHS Foundation  
Trust, London, UK.

\*Corresponding author(s). E-mail(s): [linglong.qian@kcl.ac.uk](mailto:linglong.qian@kcl.ac.uk);  
[zina.ibrahim@kcl.ac.uk](mailto:zina.ibrahim@kcl.ac.uk);

Contributing authors: [hugh.logan\\_ellis@kcl.ac.uk](mailto:hugh.logan_ellis@kcl.ac.uk);  
[ao.zhang@ndm.ox.ac.uk](mailto:ao.zhang@ndm.ox.ac.uk); [yuezhou.zhang@kcl.ac.uk](mailto:yuezhou.zhang@kcl.ac.uk); [tao.wang@kcl.ac.uk](mailto:tao.wang@kcl.ac.uk);  
[richard.j.dobson@kcl.ac.uk](mailto:richard.j.dobson@kcl.ac.uk);

## Abstract

This study presents a novel approach to addressing the challenge of missing data in multivariate time series, with a particular focus on the complexities of healthcare data. Our Conditional Self-Attention Imputation (CSAI) model, grounded in a Transformer-based framework, introduces a conditional hidden state initialization tailored to the intricacies of medical time series data. This methodology diverges from traditional imputation techniques by specifically targeting the imbalance in missing data distribution, a crucial aspect often overlooked in healthcare datasets.

By integrating advanced knowledge embedding and a non-uniform masking strategy, CSAI adeptly adjusts to the distinct patterns of missing data in Electronic Health Records (EHRs). This strategic approach not only boosts imputation

accuracy but also aligns with the inherent temporal dynamics and feature interdependencies typical in clinical data. Our model’s unique ability to capture subtle temporal relationships significantly improves data restoration efficiency.

Extensive experimental evaluations demonstrate that CSAI outperforms existing methods, particularly in managing the complexities of missing data in healthcare time series. Furthermore, we have redefined the time series interpolation task, ensuring greater alignment with clinical demands. In our commitment to collaborative advancement, the code for CSAI will be made available, facilitating further research and application in the field of healthcare analytics. The code will be made available at <https://github.com/LINGLONGQIAN/CSAI>.

**Keywords:** Conditional Knowledge Embedding, healthcare Time-series

## 1 Introduction

Multivariate time-series data, particularly from Electronic Health Records (EHRs), play a crucial role in predictive healthcare analytics [1] and a plethora of models have been designed to produce patient-specific prognoses from EHR data [2, 3]. However, EHR time-series are characterised by their complexity, and designing successful downstream predictive models requires tackling the abundance of non-random missingness of correlated variables recorded over time. Over 50% of EHR data is missing not at random, which is a result of the natural temporal irregularities in data acquisition and documentation according to healthcare and administrative decisions [4], the frequency and gaps between the recording of vital signs widely vary. For instance, while vital signs like heart rate are regularly monitored, data on white blood cell counts are often inconsistently recorded, reflecting the variable nature of healthcare decision-making. This irregularity in data collection creates a complex landscape for imputation algorithms [5].

The above challenges are further compounded by the fact that the healthcare manifestations of the same disease can vary substantially, creating additional diversity in the data [6, 7] and that healthcare variables and their missingness patterns tend to correlate over time. For instance, because hypertension is a known cause of kidney disease, EHR datasets generally show high correlations between the recording patterns of blood pressure and urine creatinine levels [8]. Retrospective studies have shown significant variation in missingness patterns across tasks, variables, and time in multi-centre medical data [4]. Traditional statistical and machine-learning imputation methods, those which make strong assumptions about the data distributions, are therefore inadequate given the complexity of the task [9–11].

Recent advancements in deep learning have shown promise in addressing these challenges, offering more sophisticated approaches to impute missing data in time-series [12–14], while the integration of domain knowledge into AI models is not just beneficial—it is essential.

It is crucial to remember that EHR data are primarily collected for healthcare care and administrative purposes [15], not specifically for research. These experts bring

a deep understanding of care practices, patient data intricacies, and the nuances of data processing, which are invaluable for insightful and accurate analysis. AI models enhanced with this level of domain expertise are not only more adept at interpreting complex medical data but also align more closely with the practicalities and subtleties of patient care.

In this work, we introduce an innovative approach to healthcare time-series missing Not At Random (MNAR) data imputation, extending the capabilities of traditional Transformer-based models. Building upon the foundation laid by the BRITS [16] architecture, our methodology integrates a novel conditional hidden state initialization mechanism with non-uniform masking strategy. This advancement is particularly focused on addressing the intricacies of temporal dynamics and feature interdependencies in time-series data.

## 2 Related Work

Efforts to impute multivariate time-series data have resulted in numerous strategies where we mainly focus on highly performing deep learning models. Among those, the GRUD model [17] incorporates temporal decay for missing data imputation, and its extensions, MRNN [18] and BRITS [16], capture temporal dynamics and missingness patterns across multiple features utilizing bidirectional RNNs. However, the MRNN model’s limitation lies in treating imputed values as constants without sufficient updates during iterations. In contrast, BRITS, free from specific data assumptions, has exhibited superior performance across domains.

Stochasticity has been introduced in RNN models in GRUU [19], variational autoencoders in V-RIN [20] and generative adversarial networks in  $E^2$ GAN [21]. However, all existing approaches require additional uncertainty modules added to the imputing network, which translates to unstable training due to increased coupling and leads to less accurate imputation [22]. CSDI [23] utilizes score-based diffusion models conditioned on observed data, explicitly trained for imputation, and capable of exploiting correlations between observed values. However, a notable concern with CSDI, as indicated in their repository, is data leakage issues similar to those in BRITS, potentially influencing the information inferred for test data.

Transformers, initially gaining prominence in natural language processing and computer vision, have been adapted for time-series analysis with notable success [24]. The TransformerEncoder, a pivotal element of these architectures, excels in capturing long-range dependencies and complex temporal patterns, thanks to its self-attention mechanism. This mechanism dynamically assesses the significance of different points in a time-series, enabling a detailed understanding of temporal relationships. SAITS [25], focusing on the MCAR (Missing Completely at Random) case, explores the capabilities of self-attention mechanisms in handling time-series imputation.

However, despite their adaptability to sequential data and effectiveness in long-range dependency modeling, Transformers face challenges specific to time-series data. A critical limitation is their inherent permutation invariance due to the self-attention mechanism, which can result in the loss of crucial temporal information. Models like NRTSI [26] have been argued to compromise parallel computational efficiency

through nested loops [25]. Addressing this issue typically involves integrating positional encodings, yet there is ongoing debate about their effectiveness in capturing fine-grained temporal nuances, particularly in scenarios with complex missing patterns and inter-feature relationships.

RDIS [27] employs ensemble learning and multiple masking strategies to boost performance, which is the same idea as  $M^3$ -BRITS [28]. Despite these advancements, a significant gap remains in integrating domain-specific knowledge, particularly from healthcare, which is crucial for interpreting and leveraging the temporal and relational intricacies of healthcare data. A critical aspect often overlooked in these models is the integration of domain knowledge, especially in healthcare. As highlighted by recent literature, EHR data are primarily collected for healthcare care and administrative functions, not explicitly for research. This nature of EHR data necessitates the involvement of domain experts who understand the intricacies of care practices and the subtleties of healthcare data processing [15]. Incorporating this knowledge into AI models is crucial for accurately interpreting and managing the unique challenges of healthcare data, such as disparate missingness distributions.

## 3 Terminology and Background

### 3.1 Incomplete Multivariate time-series representation

For a temporal interval observed over  $T$  discrete time-steps, we represent a multivariate time-series as a matrix  $\mathbf{X} = \{\mathbf{x}_1, \mathbf{x}_2, \dots, \mathbf{x}_T\}$ , composed of  $T$  observations. Each observation, denoted by  $\mathbf{x}_t \in \mathbb{R}^{1 \times D}$ , is a vector of  $D$  features. It is crucial to note that  $\mathbb{R}^D$  is heterogeneous, encompassing structured data types that extend beyond purely numerical features. This configuration allows for a comprehensive representation of the diverse data elements inherent in complex multivariate time-series.

Information related to missing values is encapsulated within two derived matrices (see Fig. 1). The mask matrix  $\mathbf{M} \in \mathbb{R}^{T \times D}$  indicates whether each element of  $\mathbf{X}$  is observed or missing:

$$m_t^d = \begin{cases} 0, & \text{if } x_t^d \text{ is missing} \\ 1, & \text{otherwise} \end{cases} \quad (1)$$

Additionally, given that the time elapsed between consecutive observations can vary across the interval, we denote the time gaps at each time step  $s_t$  as  $\delta_t$ . Given the potential for non-uniform sampling across features in the data  $\mathbf{X}$ , there is a corresponding variability in  $\delta_t$ . The  $\delta^d \in \mathbb{R}^{T \times D}$  encodes the time gap between two successive observed values for each feature  $d$ , providing an additional indicator of temporal context to the dataset. The definition of this indicator follows:

$$\delta_t^d = \begin{cases} s_t - s_{t-1} + \delta_{t-1}^d & \text{if } t > 1, m_t^d = 0 \\ s_t - s_{t-1} & \text{if } t > 1, m_t^d = 1 \\ 0 & \text{if } t = 1 \end{cases} \quad (2)$$

Time series X					Mask					Time gap					
5	/	/	8	9	1	0	0	1	1	0	4	5	7	2	$d = 1$
7	/	/	/	9	1	0	0	0	1	0	4	5	7	9	$d = 2$
2	4	1	6	/	1	1	1	1	0	0	4	1	2	4	$d = 3$
$x_1$	$x_2$	$x_3$	$x_4$	$x_5$	$m_1$	$m_2$	$m_3$	$m_4$	$m_5$	$\delta_1$	$\delta_2$	$\delta_3$	$\delta_4$	$\delta_5$	

**Fig. 1** An example of multivariate time-series. Observations  $\mathbf{x}_{1-5}$  in time-stamps  $\mathbf{s}_{1-5} = 0, 4, 5, 7, 9$ . Feature  $d_2$  was missing during  $\mathbf{s}_{2-4}$ , the last observation took place at  $\mathbf{s}_1$ . Hence,  $\delta_5^2 = t_5 - t_1 = 9 - 0 = 9$ .

## 3.2 Task definition and Implementation Bias

A large amount of existing work is carried out according to the same model or even the same implementation method, leading to the accumulation of errors or comparing performance in an unfair way, which encourages us to re-formulate tasks and point out potential risks and correct them.

### 3.2.1 Data Leakage Risk

Data normalization before dataset splitting, a common practice in models like BRITS [16] and CSDI [23], poses a significant risk of data leakage. This process often involves normalizing the entire dataset before dividing it into training, validation, and test subsets, leading to the inadvertent inclusion of validation/test set distribution information in the training dataset. Such normalization practices may result in misleadingly high-performance metrics, necessitating a reevaluation of data preprocessing methods. The entire dataset  $\mathbf{X}$  is normalized as follows before splitting into training, validation, and test sets:

$$\mathbf{X}_{\text{norm}} = \frac{\mathbf{X} - \mu(\mathbf{X})}{\sigma(\mathbf{X})} \quad (3)$$

Where  $\mu(\mathbf{X})$  and  $\sigma(\mathbf{X})$  are the mean and standard deviation of the dataset  $\mathbf{X}$ , respectively. This process leads to data leakage as the distribution characteristics of the entire dataset are used.

To prevent data leakage, normalization should ideally be performed after splitting the dataset into training  $\mathbf{X}_{Tr}$ , validation  $\mathbf{X}_{Va}$ , and test  $\mathbf{X}_{Te}$  sets:

To mitigate data leakage risk and ensure more consistent model training, the validation and test sets should ideally be normalized using the mean and standard deviation of the training set. This approach promotes smoother training by maintaining uniform data distribution, although normalization using each set’s own distribution is also viable.

### 3.2.2 Task Risk

The definition of learning tasks in time-series imputation, as exemplified by SAITS [25] with its MIT and ORT, can be overly complex. Simplifying task definitions to focus on self-supervised training with diverse artificial masks could enhance model clarity. Different masking strategies in the training set, as seen in models like BRITS and

CSDI, influence the amount and quality of observation data available for learning. A clear, uniform approach to task definition is necessary for fair comparison and effective model training.

### 3.2.3 Inadequate Masking Risk

Manual masking, a crucial step in time-series imputation models, often leads to discrepancies in mask probability. The conversion from mask probability to the number of masks is not always equivalent, causing the actual mask probability to be lower than expected. This results in an excess of observations in training, potentially diminishing the model’s actual performance compared to its reported effectiveness under a given missing rate.

## 3.3 Overview of the BRITS Backbone

BRITS [16] architecture, combining a fully-connected regression module and a recurrent component, applies temporal decay (Eq. (5)) and a decay factor to handle temporal correlations and adjust influence based on temporal distance. Missing values within an observation  $\mathbf{x}_t$  are managed via a historical representation  $\hat{\mathbf{x}}_t$  and a masking vector  $\mathbf{m}_t$ , producing a complement vector  $\mathbf{x}_t^{hc}$  that accounts for missingness patterns (Eq. (5)-(8)).

$$\mathbf{h}_0 = 0 \quad (4)$$

$$\gamma_{th} = \exp(-\max(0, \mathbf{W}_{\gamma h} \delta_t + \mathbf{b}_{\gamma h})) \quad (5)$$

$$\hat{\mathbf{h}}_{t-1} = \mathbf{h}_{t-1} \odot \gamma_{th} \quad (6)$$

$$\hat{\mathbf{x}}_t = \mathbf{W}_x \hat{\mathbf{h}}_{t-1} + \mathbf{b}_x \quad (7)$$

$$\mathbf{x}_t^{hc} = \mathbf{m}_t \odot \mathbf{x}_t + (1 - \mathbf{m}_t) \odot \hat{\mathbf{x}}_t \quad (8)$$

BRITS explores intra-observation correlations through a fully-connected layer, generating  $\mathbf{x}_t^{fc}$ , a feature-wise approximation of missing values (Eq. (9)). The concept of decay extends to feature space, resulting in a learnable factor,  $\hat{\beta}_t$ , considering both temporal decay and the masking vector (Eq. (10)-(11)). This integration produces the imputed matrix  $\mathbf{C}_t$ , effectively combining observed and imputed data (Eq. (12)-(13)).

$$\mathbf{x}_t^{fc} = \mathbf{W}_z \mathbf{x}_t^{hc} + \mathbf{b}_z \quad (9)$$

$$\gamma_{tf} = \exp(-\max(0, \mathbf{W}_{\gamma f} \delta_t + \mathbf{b}_{\gamma f})) \quad (10)$$

$$\hat{\beta}_t = \sigma(\mathbf{W}_\beta [\gamma_{tf} \circ \mathbf{m}_t] + \mathbf{b}_\beta) \quad (11)$$

$$\mathbf{x}_t^c = \beta_t \odot \mathbf{x}_t^{fc} + (1 - \beta_t) \odot \mathbf{x}_t^{hc} \quad (12)$$

$$\mathbf{C}_t = \mathbf{m}_t \odot \mathbf{x}_t + (1 - \mathbf{m}_t) \odot \mathbf{x}_t^c \quad (13)$$

$$\mathbf{h}_t = \sigma(\mathbf{W}_t \hat{\mathbf{h}}_{t-1} + \mathbf{U}_h [\mathbf{C}_t \circ \mathbf{m}_t] + \mathbf{b}_h) \quad (14)$$

The final step (Eq. (14)) updates the hidden state via Recurrent Neural Networks (RNNs), leveraging various indicators to learn functions of past observations. The

bidirectional recurrent dynamics approach integrates backward information to tackle slow convergence.

In essence, BRITS exploits temporal and feature correlations in multivariate time-series data, employing decay factors, a regression module, and a bidirectional RNN for imputing missing values. The final hidden states are updated using imputations and corresponding masks, with the integrated processes visualized in Figure 2.

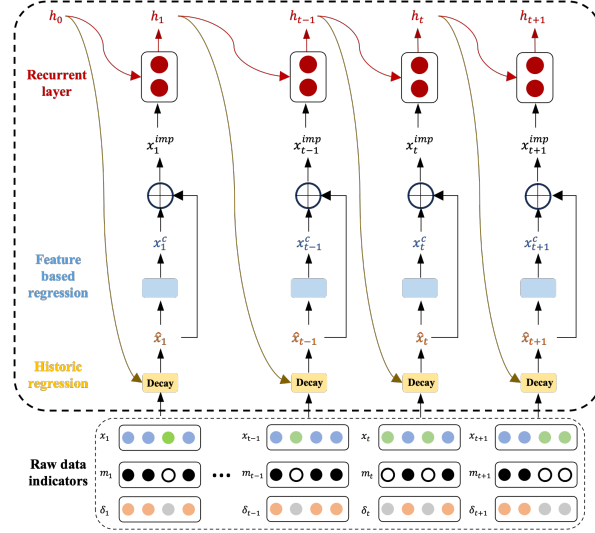


Fig. 2 The backbone processes of BRITS

## 4 Methodology

In this section, we introduce a novel approach: Transformer-based Conditional Hidden State Initialization, along with Non-Uniform Masking. This method is an extension and enhancement of the BRITS architecture, tailored to address specific challenges in healthcare time-series data imputation, as illustrated in 3.

### 4.1 Non-Uniform Masking Strategy

Our non-uniform masking strategy fundamentally diverges from traditional approaches by leveraging the inherent missing distribution characteristic of each feature. This strategy is predicated on the principle that the probability of missingness in healthcare data is not uniformly distributed across all features. Instead, it varies based on specific healthcare parameters and patient conditions. By incorporating this variability into our masking process, we aim to create a more realistic and representative model of the missing data patterns encountered in healthcare settings.

The core of our algorithm involves generating non-uniform masking probabilities, guided by regulatory factors that account for the unique missing distribution of each

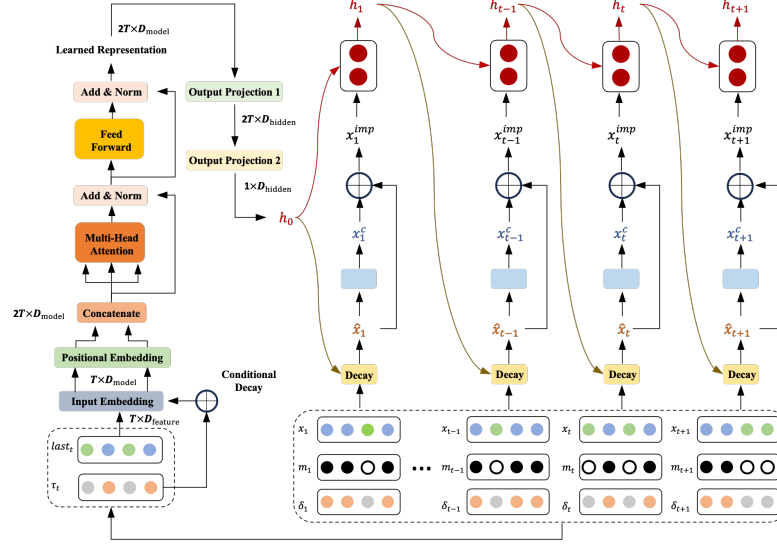


**Fig. 3** The Conditional Self-Attention Hidden State Initialization Procedure. The architecture commences with an Input Embedding layer that transforms raw data inputs into a dense representation. This is followed by Positional Embedding, which injects temporal information, ensuring that the model can discern the sequence of events within the time-series. The embeddings are then concatenated, forming a comprehensive input that encapsulates both the data and its temporal context.

feature. Another essential aspect is the manual adjustment factor, designed to fine-tune the masking process. This factor is adaptively set based on the observation frequency per feature, allowing for a tailored masking strategy. This adaptive approach strikes a balance between avoiding overfitting in sparse data scenarios and ensuring sufficient learning signals in data-rich contexts. It is designed to optimize the model's ability to discern underlying patterns and relationships, enhancing its predictive accuracy and generalization across diverse healthcare data patterns. For a given feature  $d$ , the non-uniform masking probability  $P_{\text{nu}}(d)$  is determined as follows:

$$Q_{\text{mask}}(d|U, I) = F(d, U, I) \quad (15)$$

$$P_{\text{nu}}(d) = Q_{\text{mask}}(f) \times P_{\text{dist}}(d) \quad (16)$$

Where:

- $U$  and  $I$  are the pre-defined parameters.
- $Q_{\text{mask}}(d|U, I)$  is the regulatory factor for feature  $d$ , conditioned by  $U$  and  $I$ .
- $P_{\text{dist}}(d)$  represents the probability distribution of missingness for feature  $d$ .

The overall masking proportion is then adjusted to ensure consistency with the uniform masking rate  $U$ , while retaining the non-uniform characteristics of the individual features. The pseudocode for this algorithm is as follows:



---

**Algorithm 1** Non-Uniform Masking Strategy

---

**Require:** Dataset  $\mathbf{X}$  with  $D$  features, Uniform masking rate  $U$ , Adjust factor  $I$

**Ensure:** Masked Dataset  $\mathbf{X}_M$

- 1: Missing distribution  $\mathbf{P}_{\text{dist}}$  for feature  $d$
  - 2: **for each** feature  $d$  in  $D$  **do**
  - 3:     Determine regulatory factor  $R_{\text{factor}}(d)$  based on  $\mathbf{P}_{\text{dist}}(d)$  and adjust factor  $I$
  - 4:     Generate non-uniform masking probabilities  $\mathbf{P}_{\text{nu}}(d)$  for  $d$  using  $R_{\text{factor}}(d)$
  - 5: **end for**
  - 6: Readjust  $\mathbf{P}_{\text{nu}}$  across all features to match target overall masking rate  $U$
  - 7: Apply  $\mathbf{P}_{\text{nu}}$  to  $D$  to create masked dataset  $\mathbf{X}_M$
- 

## 4.2 Conditional Knowledge Embedding

In healthcare practice, much like the observer effect in physics, the process of recording medical data can have a significant impact on the patient’s condition, especially in the case of invasive tests. This parallel underscores the critical nature of timing in healthcare measurements, where the relevance of historical observations is often contingent on the elapsed time since their occurrence. The last observation of a patient’s status and the median time gap between these observations are pivotal in accurately understanding the patient’s current condition. Careful timing, akin to precise measurement in physics, is essential to minimize the impact on the patient and to ensure the accuracy of the data collected.

In response to this healthcare necessity, we introduce a decay attention mechanism that dynamically adjusts the attention weight based on the time gap between observations. This innovative approach, informed by healthcare domain knowledge, recognizes the crucial role of temporal proximity in the diagnostic value of data points. By prioritizing recent observations and accounting for the natural variability in healthcare data collection, our decay attention method aligns with the realities of healthcare practice, enhancing the predictive capabilities of time-series analysis in healthcare settings.

**Decay Function Formulation.** Different with the BRITS architecture, our decay attention function  $A(\delta_t)$  introduces a nuanced approach. It is used to represent the attention weight assigned to an observation at time  $t$ . This function diminishes as the time gap  $\delta_t$ . The function is expressed as:

$$A(\delta_t) = \exp(-\alpha(\delta_t)) \tag{17}$$

where  $\alpha$  denotes a decay rate parameter or a learnable neural network that modulates how rapidly the attention weight decreases with time.

This decay attention mechanism effectively encapsulates the healthcare intuition that more recent observations carry greater diagnostic value. By embedding this temporal knowledge into the neural network, the model becomes more aligned with healthcare realities, thereby enhancing its predictive capabilities in healthcare applications.

**Integration of Median Time Gap.** To enhance the model’s healthcare applicability, we have integrated the median time gap  $\tau$  for a specific healthcare feature.

This integration leads to a tailored adjustment, giving more weight to observations closer to the median time gap and less to those further away. This adjusted function is formulated as:

$$A_{\text{adjusted}}(\delta_t, \tau) = \exp(-\alpha(\delta_t - \tau)) \quad (18)$$

This ensures that the attention peaks when the time gap  $\delta_t$  closely approximates the median  $\tau$ , and declines as the discrepancy between  $\delta_t$  and  $\tau$  widens.

**Challenges in Implementation.** Implementing the decay attention model within a neural network framework presents significant challenges, particularly in maintaining consistency between the signs of the input and output values following nonlinear transformations. Avoiding direct application of absolute value functions on the output is critical, as such operations can interfere with the network’s training dynamics by disrupting the gradient flow. This, in turn, could lead to unstable or ineffective learning processes during model training.

#### 4.2.1 Transformer-based hidden state initialization

In the realm of time-series data analysis, BRITS (Bidirectional Recurrent Imputation for time-series) represents a significant advancement, leveraging recurrent neural networks to adeptly handle missing values in multivariate time-series. Its architecture, characterized by bidirectional dynamics and a novel application of decay factors, addresses the challenge of temporal correlations with a level of sophistication unmatched by traditional methods.

However, despite its robustness, BRITS has certain limitations in capturing intricate temporal and feature correlations, particularly in highly dynamic environments. Our research extends the BRITS framework, focusing on conditional hidden state initialization. This enhancement allows for a more nuanced understanding of temporal dynamics, offering improved performance in scenarios where the temporal relationship between data points is especially critical. That is acutely aware of the underlying temporal patterns in the data, which is particularly relevant in fields like healthcare, where the timing of events can be as crucial as the events themselves.

**Conditional Self-Attention Hidden State Initialization.** The cornerstone of our method lies in the initialization of hidden states. Unlike BRITS, which initializes hidden states with zeros, our approach leverages the last observed data point and a decay attention mechanism to generate the proper conditional hidden state distribution  $q(\mathbf{h}_{\text{init}} | \mathbf{x}_{\text{last\_obs}}, \mathbf{A}_{\text{adjusted}}(\delta_t, \tau))$  with the model distribution  $p_{\theta}(\mathbf{x}_t)$ . This strategy is designed to provide a more contextually rich starting point for the model, thus enhancing the effectiveness of subsequent imputations.

In contrast to the general decay in BRITS, where the decay factor is applied directly to the previous hidden state 6 and 10, our approach uses the decay factor to modulate the attention mechanism. This modification allows for a more fine-grained and feature-specific understanding of temporal relationships within the data, enhancing the model’s ability to adapt to varying temporal dynamics across different healthcare features.

**Input Projection and Positional Encoding.** At each time step  $s_t$ , the last observation  $\mathbf{x}_{\text{last\_obs}} \in \mathbb{R}^{N \times T \times D_{\text{feature}}}$  from input time-series data  $\mathbf{x}_t$  undergo transformation alone with  $\mathbf{A}_{\text{adjusted}}(\delta_t, \tau) \in \mathbb{R}^{N \times T \times D_{\text{feature}}}$  from 18. The Positional Encoding module and an Input Projection module are used to transform them into  $\mathbb{R}^{N \times T \times D_{\text{model}}}$ , defined as:

$$\mathbf{x}'_{\text{last\_obs}} = \text{PosEncoder}(\text{InputProj}(\mathbf{x}_{\text{last\_obs}})) \quad (19)$$

$$\mathbf{A}'_{\text{adjusted}}(\delta_t, \tau) = \text{PosEncoder}(\text{InputProj}(\mathbf{A}_{\text{adjusted}}(\delta_t, \tau))) \quad (20)$$

**Transformer enhancement.** The concatenated input for the Transformer Encoder  $\mathbf{C}_{\text{in}}$  is formed by combining transformed last observation and decay attention and processed through multiheaded self-attention (MSA), layernorm (LN), and feed-forward networks (FFN).

$$\mathbf{C}_{\text{in}} = \text{Concat}(\mathbf{x}'_{\text{last\_obs}}, \mathbf{A}'_{\text{adjusted}}(\delta_t, \tau)) \quad (21)$$

$$\mathbf{C}_{\text{out}} = \text{LN}(\text{FFN}(\text{LN}(\text{MSA}(\mathbf{C}_{\text{in}})))) \quad (22)$$

**Information Scaling to initialize Hidden State.** The enhanced output of Transformer Encoder is scaled to the dimensions required by the hidden state  $\mathbf{h}_{\text{init}}$  through alternating 1D convolution.

$$\mathbf{H}_1 = \text{Conv1}_1(\mathbf{C}_{\text{out}} * \mathbf{W}_1 + \mathbf{b}_1) \quad (23)$$

$$\mathbf{h}_{\text{init}} = \text{Conv1d}_2(\mathbf{H}_1 * \mathbf{W}_2 + \mathbf{b}_2) \quad (24)$$

where 23 transform  $\mathbf{C}_{\text{out}}$  from  $\mathbb{R}^{N \times L \times d_{\text{model}}}$  to  $\mathbb{R}^{N \times L \times d_{\text{hidden}}}$  and produces  $\mathbf{H}_1$ , 24 further scale  $\mathbf{H}_1$  to  $\mathbb{R}^{N \times 1 \times d_{\text{hidden}}}$  to generate the initialized Hidden State  $\mathbf{h}_{\text{init}}$ .

## 5 Experiments

For the sake of the reproducibility of our results, we make our work publicly available to the community. Our data preprocessing scripts, model implementations, and hyperparameter search configurations are all available in the GitHub repository.

In this study, we rigorously evaluate the performance of our Conditional Self-Attention Imputation (CSAI) model against a selection of state-of-the-art baselines in the context of four real-world healthcare datasets. Our comparison includes an array of established models: BRITS, BRITS-GRU, GRUD, V-RIN(full), and MRNN. It’s important to note that we specifically include BRITS-GRU as a baseline due to the original BRITS model utilizing LSTM cells, while other baselines employ GRU cells. This addition ensures a fair and comprehensive comparison across similar architectures.

For each experimental setup, we select only the best-performing model from each baseline study for a more focused and meaningful comparison. Although a comparison with  $E^2\text{GAN}$  would have provided additional insights, especially since it did not quantitatively compare it with BRITS. The publicly available implementation of  $E^2\text{GAN}$

is unfortunately incompatible with our current setup, precluded the possibility of directly comparing  $E^2$ GAN with other models in our evaluation.

## 5.1 Datasets

Each of the four datasets chosen for experimental evaluation has a different data distribution, especially the MIMIC-III database, from which we extracted two different datasets to model different tasks. We reproduced the benchmarking papers for these public datasets, skipping steps that remove all-NAN samples to retain the data with its original missingness.

1. **eICU** [29] is sampled from the eICU Collaborative Research Database, a multi-center database with anonymised hospital patient records. eICU is publicly available after registration, including completion of a training course in research with human subjects and signing of a responsible data use agreement <sup>1</sup>. We followed the only benchmarking extract available for eICU.
2. **MIMIC-III**<sup>2</sup> [30] is an extensive, freely-available database of over 40,000 critical care patients. To complement our MIMIC experiments with heterogeneous feature types and data dimensionality, we followed two benchmark papers [31, 32] and extracted different datasets for the experiment. 14,188 samples for 89 variables; 21,128 valid samples with 59 variables.
3. **PhysioNet Challenge 2012 dataset**. The Predicting Mortality of ICU Patients: The PhysioNet/Computing in Cardiology Challenge 2012, a public medical benchmarking dataset provided by [33], contains records of 4000 48-hour ICU stays, allowing unbiased evaluations of different model performances. 3,997 samples with 35 variables.

## 5.2 Implementation Details

We trained our models on an HPC node with NVIDIA A100 40GB running Ubuntu 20.04.6 LTS (Focal Fossa). We used Python: 3.8.16. All package details can be found in our repository. For each of the five datasets, we created three versions by further masking 5%, 10% and 20% cells in addition to the missingness already present in the original datasets. These masked cells have known ground truths and will form the basis of our comparison of imputation performance.

We used the Adam optimizer for training and set the number of RNN hidden units to 108 for all models. The batch size is 64 for PhysioNet and traffic data and 128 for the other datasets. To promote stable training, each dataset was normalized to have zero mean and unit variance. Randomly, we selected 10% of each dataset for validation and another 10% for testing, training the models on the remaining data. For the imputation task, we randomly masked 10% of observations in each dataset to serve as the ground truth, which was used as validation data. A 5-fold cross-validation method was implemented to evaluate the models. Imputation performance was gauged using the Mean Absolute Error (MAE) and Mean Relative Error (MRE). As for the

---

<sup>1</sup><https://physionet.org/content/eicu-crd/2.0/>

<sup>2</sup><https://physionet.org/content/mimiciii/1.4/>

non-uniform masking strategy, we conducted a detailed analysis. For fair analysis with other works, we only adopt this strategy for the training set in all datasets.

### 5.3 Experimental Results

The consolidated analysis of both imputation and classification tasks, as reflected in the experimental results, underscores the strengths and areas for improvement of the Conditional Self-Attention Imputation (CSAI) model across various healthcare datasets.

The performance of our Conditional Self-Attention Imputation model (CSAI) across different datasets and masking ratios demonstrates notable efficacy in the imputation task. As indicated in Table 1, CSAI consistently achieved the lowest Mean Absolute Error (MAE), outperforming traditional models like BRITS, BRITS-GRU, and others. This is particularly evident at lower masking ratios on both the eicu and mimic\_59f datasets, suggesting that CSAI effectively leverages limited data to accurately impute missing values. This strength underscores the model’s capability to integrate domain-specific knowledge into its architecture, adapting to the heterogeneity of medical time series data.

Table 2 reflects CSAI’s robust classification capabilities, with competitive Area under the ROC Curve (AUC) scores across various masking ratios. It demonstrates the Conditional Self-Attention Imputation (CSAI) model’s overall effectiveness, with notable performance in the eICU, PhysioNet, and MIMIC\_59f datasets. This superior performance, especially notable in the PhysioNet dataset, CSAI’s effectiveness in handling the complex task of predicting outcomes based on imputed data. However, in the MIMIC\_89f dataset, CSAI is slightly underperformed compared to BRITS-GRU. It not only indicates the robustness of the BRITS architecture and underscores the strength of the BRITS framework; but also validates its selection as the foundational structure for the CSAI model. The slightly lower performance in the MIMIC\_89f dataset could be due to various factors, such as the inherent complexity of the dataset or specific nuances in missing data patterns that might require additional model tuning.

Our comprehensive experimental evaluation of the Conditional Self-Attention Imputation (CSAI) model across diverse healthcare datasets demonstrates its effectiveness in addressing both imputation and classification tasks. CSAI’s adaptability to the complexities inherent in healthcare data, evidenced by its consistent performance across varying masking ratios, highlights its resilience to data sparsity. This is a significant advantage in real-world healthcare scenarios where incomplete data is a common challenge. The integration of domain-specific knowledge and the implementation of sophisticated imputation strategies in CSAI significantly contribute to its robustness, emphasizing the necessity of tailored approaches in the realm of healthcare analytics.

Despite the overall strong performance of CSAI, there are areas where CSAI’s performance indicates room for improvement. In the MIMIC\_89f dataset, CSAI slightly lags behind BRITS-GRU, suggesting that further model refinement is needed. This disparity opens up avenues for future research, particularly in enhancing CSAI’s domain knowledge integration mechanisms and exploring the potential benefits of additional training data. Such refinements could improve CSAI’s robustness and effectiveness across various healthcare datasets, each with its unique characteristics and challenges.

**Table 1** Comparative MAE performance of various models across different masking ratios on four datasets in imputation tasks.

	eICU (MAE_Factor)			MIMIC_59f (MAE_Factor)		
	5	10	20	5	10	20
	BVRIN	0.2416066624555839(0)	0.2425388767962918(0)	0.2521443794081134(0)	0.1545748298302925(0)	0.1381774096223719(0)
BRITS	0.2407022338003594(10)	0.2497367276263675(10)	0.2908578411028444(10)	0.2092907759841963(10)	0.221978248760044(10)	0.4436697924374182(10)
BRITS_GRU	0.166906016914658(0)	0.1705338739259578(0)	0.1768139684914781(0)	0.1519486919882992(0)	0.1402299219611225(0)	0.3403944741631409(0)
GRUD	0.173298982996181(10)	0.181459582420475(10)	0.1912545113021268(10)	0.196428028638464(10)	0.1975565142341144(10)	0.4088558909512462(10)
MRNN	0.172319898527054(0)	0.1712448390578215(0)	0.1769143760391551(0)	0.1479284907740569(0)	0.1419320843095624(0)	0.3416945429830419(0)
CSAI	0.1718744828009491(10)	0.1778442247114985(10)	0.1888710608272489(10)	0.1956644353841923(10)	0.193829531836644(10)	0.406053517028324(10)
	0.2227370102738632(0)	0.2256000191395106(0)	0.230979583607369(0)	0.3044727329354487(0)	0.2870424025309634(0)	0.486696332628005(0)
	0.2227370099294914(10)	0.2256000191256016(10)	0.230979583571353(10)	0.286242507254541(10)	0.245623000577053(10)	0.3932243713993742(10)
	0.4703575678949254(0)	0.4799816897156928(0)	0.500653906796392(0)	0.305728740144034(0)	0.2834192980232279(0)	0.471981224131871(0)
	0.4705992472964637(10)	0.4802804836598145(10)	0.50666473601925396(10)	0.3121194026314546(10)	0.309067721285424(10)	0.501811866549688(10)
	0.15196681888527218(0)	0.1614887565608259(0)	0.1663724494172825(0)	0.1311938059021705(0)	0.1129106347274659(0)	0.3097617904193939(0)
	0.1642066666666666(10)	0.1694361645200429(10)	0.1735980736734645(10)	0.1614537769188592(10)	0.156771998605634(10)	0.3646513545945805(10)
PhysioNet (MAE_Factor)						
	eICU (MAE_Factor)			MIMIC_89f (MAE_Factor)		
	5	10	20	5	10	20
	BVRIN	0.261627214279973(0)	0.2737156899792313(0)	0.2990655482813624(0)	0.2802916356976231(0)	0.2981212480367007(0)
BRITS	0.2612648092011688(10)	0.2730541358490472(10)	0.296735123154796(10)	0.2806728497695169(10)	0.290823365474281(10)	0.3277709622113093(10)
BRITS_GRU	0.2563447937357114(0)	0.2676201849978777(0)	0.2872153778145618(0)	0.2846978765928573(0)	0.306357803540231(0)	0.3298037457677614(0)
GRUD	0.2547109129418157(10)	0.266306516804449(10)	0.283761902727029(10)	0.2859043627187573(10)	0.3083014770071408(10)	0.3349183688979488(10)
MRNN	0.2512872199774503(0)	0.2621551395257828(0)	0.2828282523984457(0)	0.2833476946520711(0)	0.3020169393252264(0)	0.3257972313281(0)
CSAI	0.2497634140971796(10)	0.258989211587254(10)	0.273548870673468(10)	0.283609676674445(10)	0.304112929707543(10)	0.3245221556395175(10)
	0.494028434272698(0)	0.4977919324800742(0)	0.509515400807895(0)	2.162001471223608(0)	2.226354328684297(0)	2.300878604115324(0)
	0.494034032734074(10)	0.497752244641804(10)	0.5099663862514093(10)	2.167760678286366(10)	2.23570174355051(10)	2.321214564671742(10)
	0.546711967567588(0)	0.556476306450407(0)	0.5729252103217068(0)	0.5077789122169134(0)	0.5202164923417467(0)	0.534089506750974(0)
	0.5473808040883774(10)	0.5572730906196675(10)	0.5792898003894609(10)	0.5072132501647532(10)	0.5203111806728977(10)	0.534314937233369(10)
	0.246018259469532(0)	0.257474476838776(0)	0.2747586037341377(0)	0.284518757872656(0)	0.2984590455884935(0)	0.32777313249246507(0)
	0.2459415419362783(10)	0.2566331381409447(10)	0.2744194368336484(10)	0.284847941557604(10)	0.2989379066597622(10)	0.3349269724645914(10)

**Table 2** AUC performance comparison of CSAI and baseline models across varying masking ratios on four datasets in the classification task.

	eICU (AUC_Factor)			MIMIC_59f (AUC_Factor)		
	5	10	20	5	10	20
	BVRIN	0.8876632792674032(0)	0.8842207935257471(0)	0.8846083295889055(0)	0.8327985224797132(0)	0.8331225972961287(0)
BRITS	0.8833459136956671(10)	0.881934198142275(10)	0.8810882005813483(10)	0.830776322899148(10)	0.8301506383198871(10)	0.8245590286971046(10)
BRITS_GRU	0.8866858256973604(0)	0.885210557201445(0)	0.8856887012643835(0)	0.8282097938406451(0)	0.8277898698471445(0)	0.8241398505928232(0)
GRUD	0.8858976145705622(10)	0.885467509841966(10)	0.885933757814677(10)	0.8254673610604841(10)	0.8255691464334976(10)	0.818359801297295(10)
MRNN	0.880446123008171(0)	0.8866442109252388(0)	0.886053124480183(0)	0.831875457867805(0)	0.830741815613582(0)	0.826876535083795(0)
CSAI	0.8884366666666666(10)	0.8858544332092004(10)	0.8863321462371248(10)	0.832118215068270(10)	0.8300872854458495(10)	0.8237612852706355(10)
	0.8649908677163975(0)	0.8645586279780326(0)	0.8580064406861503(0)	0.8276771341543487(0)	0.826396052547089(0)	0.8230358085344909(0)
	0.8615153273690657(10)	0.8652561827886703(10)	0.857105197414398(10)	0.8272730300280693(10)	0.8258475229000654(10)	0.8170619548987426(10)
	0.8778555135764312(0)	0.8762569153075001(0)	0.873418789382206(0)	0.8210628460196878(0)	0.817071816803729(0)	0.8128184260363562(0)
	0.874096807875258(0)	0.8755649076047811(10)	0.8739341474938707(10)	0.819520893766984(0)	0.8191086246235789(10)	0.7999713683411305(10)
	0.8805208094995246(0)	0.8897650378954041(0)	0.8879479677632803(0)	0.8352381478170342(0)	0.8336724124061122(0)	0.8310903756879437(0)
	0.8880503633414845(10)	0.8882202129602428(10)	0.8862824221267139(10)	0.8347414542270188(10)	0.8330956316340254(10)	0.8262743541111952(10)
PhysioNet (AUC_Factor)						
	eICU (AUC_Factor)			MIMIC_89f (AUC_Factor)		
	5	10	20	5	10	20
	BVRIN	0.834350245783333(0)	0.8291631265561537(0)	0.8254836447961708(0)	0.8515838497027204(0)	0.8483391172226782(0)
BRITS	0.8293967729758774(10)	0.8267641858832944(10)	0.8263446793122851(10)	0.8495210570941497(10)	0.843096708552293(10)	0.839207436622788(10)
BRITS_GRU	0.822140767045229(0)	0.81175067602856(0)	0.8218051204357302(0)	0.8518059085347305(0)	0.8499103429115371(0)	0.8410220558148127(0)
GRUD	0.8192386703530378(10)	0.815668320922555(10)	0.808384303486773(10)	0.849614080231907(10)	0.8447876540359719(10)	0.8411338665078617(10)
MRNN	0.8067688302396302(0)	0.8192578961191943(0)	0.8065060341956709(0)	0.854103082599695(0)	0.8520571833345272(0)	0.8430684026521217(0)
CSAI	0.8162466418317044(10)	0.815696279484991(10)	0.811000785750067(10)	0.8546523670183401(10)	0.8528274217295089(10)	0.8433371049261502(10)
	0.78997442809062(0)	0.7765171413166387(0)	0.7698864925325907(10)	0.7924280641870158(0)	0.789628259467959(0)	0.7732159684544777(0)
	0.7931826963958326(10)	0.7870501888977707(10)	0.7649544009174021(10)	0.7950260265800328(10)	0.7899081915853703(10)	0.7819922487688943(10)
	0.8012121900939138(0)	0.7994518346019279(0)	0.7939973744164519(0)	0.828283355107209(0)	0.8308854640080671(0)	0.823715692404899(0)
	0.7951155893101695(10)	0.7996707646193981(10)	0.7873419297547143(10)	0.8323709476437614(10)	0.8287261378778332(10)	0.8179165273816347(10)
	0.8646453089244852(0)	0.8591914569031273(0)	0.8372234935163996(0)	0.837759164790705(0)	0.8400507785337318(0)	0.8317807876933676(0)
	0.865496313246886(10)	0.8652428171878973(10)	0.8609585558098145(10)	0.8410557504273509(10)	0.8409539757561252(10)	0.8281903435998187(10)

## 5.4 Ablation Study

### 5.4.1 Non-uniform masking strategy Comparison

In this ablation study, we examine the efficacy of our proposed non-uniform masking strategy across different data partitions: training, validation, and test sets. To ensure a fair comparison, we implemented the same validation and test settings as in the existing literature, alongside our non-uniform masking variant. The different permutations examined include:

- **Train only:** Non-uniform masking applied solely to the training set.
- **All:** Non-uniform masking applied across all data sets.
- **None:** A baseline with no non-uniform masking.

- **Val only:** Non-uniform masking applied only to the validation set.
- **Val Test:** Non-uniform masking applied to both the validation and test sets.
- **Test only:** Non-uniform masking applied exclusively to the test set.

We utilized the BRITS and BRITS-GRU models for this comparison. The "All" configuration emerged as the top performer, suggesting that our non-uniform masking strategy, when applied uniformly across all data partitions, optimally leverages the data's distribution to improve learning.

Our findings reveal that the "All" permutation of non-uniform masking yields the best performance. This indicates that a consistent application of our masking strategy across training, validation, and test sets can effectively adjust the proportion of different features, accommodating their varied learning difficulties and improving the model's overall ability to handle the missingness inherent in medical time-series data.

Table 3 summarizes the performance metrics of each permutation, demonstrating the comparative improvements achieved with the "All" configuration. The observed performance gains validate our hypothesis that a non-uniform masking strategy enhances the model's capacity to handle the data's heterogeneous nature.

**Table 3** Performance Comparison Across Non-Uniform Masking Permutations. This table presents a detailed analysis of the impact of different non-uniform masking strategies on both imputation and classification tasks, using the BRITS and BRITS-GRU models. The 'All' configuration, where non-uniform masking is applied across training, validation, and test sets, consistently demonstrates superior performance, emphasizing the effectiveness of a uniform application of the strategy.

Model	Masking	Imputation		Classification		
		Epoch	MAE	Epoch	MAE	AUC
Brits	All	182.2	<b>0.234929</b>	28.6	0.262997	<b>0.819142*</b>
	Val_Test	187	0.235739	57	0.262268	0.816184
	Test_only	218.6	0.236001	61.6	0.265496	0.813821
	Train_only	215.8	0.266307	25.4	0.310624	0.815686
	None	218.6	0.26762	61.6	0.313257	0.81175
	Val_only	187	0.268386	57	0.309332	0.818605
Brits-GRU	All	294.8	<b>0.231594</b>	21.8	0.26615	0.811869
	Val_Test	287.4	0.233243	21.6	0.267872	0.813855
	Test_only	286	0.23363	15.4	0.270678	<b>0.821355*</b>
	Train_only	288.4	0.258989	17.6	0.313681	0.815697
	Val_only	287.4	0.262149	21.6	0.314871	0.81071
	None	286	0.262155	15.4	0.318493	0.819258

#### 5.4.2 Adjustment Factor Comparison

The experimental results depicted in the table indicate a nuanced relationship between the adjustment factor in the non-uniform masking strategy and the performance on imputation and classification tasks. An optimal adjustment factor demonstrated to be around 5, results in the lowest imputation error, suggesting that a balanced representation of features is crucial for accuracy. For classification, however, increasing the

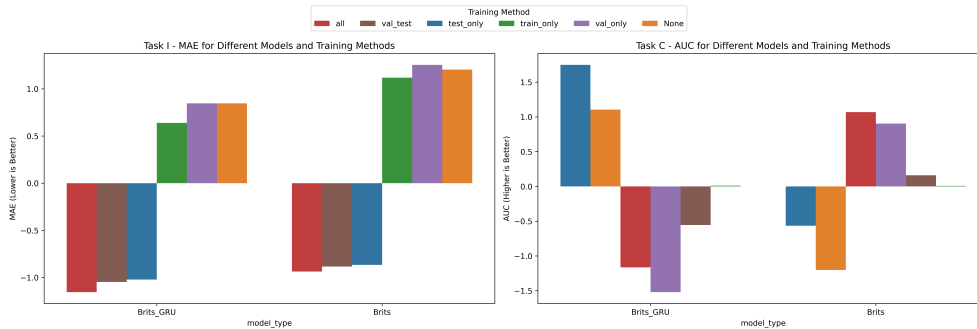


**Fig. 4** Visualization of Performance Variations in the Physionet Dataset Across Different Masking Strategies. This figure illustrates the comparative effectiveness of various masking permutations on the Physionet dataset, highlighting how each strategy influences the model’s performance in terms of MAE, and AUC.

adjustment factor leads to higher errors and a marginal decline in AUC, highlighting that excessive weighting may not uniformly enhance performance across different machine-learning tasks. These findings reveal the delicate interplay between feature representation adjustments and task-specific model efficacy, underscoring the importance of calibration in the non-uniform masking approach for complex time series data.

**Table 4** Impact of Adjustment Factor on Imputation and Classification Performance Metrics. The table showcases the number of epochs required and the Mean Absolute Error (MAE) for imputation, as well as the Area Under the Curve (AUC) for classification, across varying levels of the adjustment factor.

Factor	Imputation		Classification		
	Epoch	MAE	Epoch	MAE	AUC
0	286	0.26215514	15.4	0.31849296	0.8192579
5	291.2	0.2310647	33.8	0.26586726	0.80975966
10	294.8	0.23159396	21.8	0.26615049	0.8118691
50	293	0.24170042	16.4	0.28670924	0.81583396
100	285.8	0.26885496	14.2	0.32437366	0.81381879
150	283.8	0.29943347	16.6	0.35346112	0.8144707
200	289.2	0.33235399	15.6	0.39360851	0.81173828

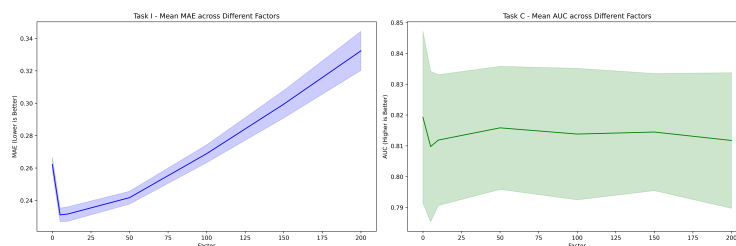


**Fig. 5** Impact of Adjustment Factor on Model Performance in the Physionet Dataset.



### 5.4.3 Implementation Comparison

The experimental results 5 highlight a significant discrepancy between reported and actual performance due to the implementation nuances of masking strategies. For both BRITS and BRITS-GRU models, the Mean Absolute Error (MAE) is notably lower in the 'Incorrected' implementation across all masking ratios compared to the 'Corrected' approach. This suggests that the initial, incorrect implementation artificially inflated the models' performance metrics. Specifically, the 'Incorrected' implementation underrepresents the masking ratio, leading to less masked data during training and, consequently, higher performance. Upon correction, the MAE values rise, reflecting a more accurate depiction of model efficacy in the presence of higher data sparsity. This discrepancy underscores the critical importance of meticulous implementation practices to avoid overestimating model capabilities in handling missing data within time series. We have attached the core of the implementation code in the appendix A.

**Table 5** Comparative Analysis of Model Performance with Incorrect vs. Corrected Masking Implementation. This table presents the MAE across different masking ratios for the BRITS and BRITS-GRU models, contrasting the performance before and after implementation corrections.

Model	MAE	Mask_Ratio	Implementation
BRITS	0.2518878	5	Incorrected
	0.2629484	10	
	0.282754	20	
	0.256344794	5	Corrected
	0.267620185	10	
	0.287215378	20	
BRITS_GRU	0.247725	5	Incorrected
	0.2564158	10	
	0.2772394	20	
	0.25128722	5	Incorrected
	0.26215514	10	
	0.282882052	20	

## 6 Discussion and Conclusions

This study has introduced a novel approach to the imputation and classification of missing data in multivariate medical time series. CSAI has demonstrated its potential to significantly improve the accuracy and reliability of medical data analysis, which is essential for high-stakes healthcare decisions.

Our comprehensive experimental evaluation has provided significant insights into the efficacy of Conditional Self-Attention Imputation (CSAI) across various healthcare datasets and scenarios of missing data. While CSAI showcased promising results, surpassing established benchmarks in many instances, it is crucial to acknowledge the challenges observed with increased data sparsity, particularly in the physionet and mimic\_89f datasets at a 20% masking ratio.

Future work should also explore the incorporation of more granular medical knowledge, potential model enhancements to better capture long-range dependencies, and techniques to handle extreme cases of missing data. Additionally, the open-source

nature of our approach encourages collaboration and iterative improvement from the research community, which is crucial for advancements in this domain.

## 7 Acknowledgments

This paper represents independent research funded by the NIHR Maudsley Biomedical Research Centre at South London and Maudsley NHS Foundation Trust and King's College London. The views expressed are those of the author(s) and not necessarily those of the NIHR or the Department of Health and Social Care. The work of Linglong Qian was supported by the Kings-China Scholarship Council PhD Scholarship Programme (K-CSC) under Grant CSC202008060096. All experiments are implemented on CREATE HPC.<sup>3</sup>

## 8 Data availability

The datasets generated and/or analyzed during the current study are available from the corresponding author on reasonable request.

## 9 Ethics declarations

### 9.1 Conflict of interest

The authors declare no conflict of interest regarding the publication of this paper.

## Appendix A Masking implementation

```
import numpy as np
if removal_percent != 0:
    # randomly eliminate 10% values as the imputation ground-truth
    indices = np.where(~np.isnan(data))[0].tolist()
    indices = np.random.choice(indices, len(indices) * removal_percent // 100)
    data[indices] = np.nan
```

Fig. A1 The original mask implementation

```
import numpy as np
if removal_percent != 0:
    # randomly eliminate 10% values as the imputation ground-truth
    random_matrix = np.random.rand(*data.shape)
    data[(~np.isnan(data)) & (random_matrix < (removal_percent))] = np.nan
```

Fig. A2 The corrected mask implementation

---

<sup>3</sup>King's College London. (2022). King's Computational Research, Engineering and Technology Environment (CREATE). Retrieved March 2, 2022, from <https://doi.org/10.18742/rnvf-m076>

## References

- [1] Ayala Solares, J.R., Diletta Raimondi, F.E., Zhu, Y., Rahimian, F., Canoy, D., Tran, J., Pinho Gomes, A.C., Payberah, A.H., Zottoli, M., Nazarzadeh, M., Conrad, N., Rahimi, K., Salimi-Khorshidi, G.: Deep learning for electronic health records: A comparative review of multiple deep neural architectures. *Journal of Biomedical Informatics* **101**, 103337 (2020)
- [2] Ibrahim, Z.M., Bean, D., Searle, T., Qian, L., Wu, H., Shek, A., Kraljevic, Z., Galloway, J., Norton, S., Teo, J.T.H., Dobson, R.J.: A knowledge distillation ensemble framework for predicting short- and long-term hospitalization outcomes from electronic health records data. *IEEE Journal of Biomedical and Health Informatics* **26**(1), 423–435 (2022) <https://doi.org/10.1109/JBHI.2021.3089287>
- [3] Shamout, F.E., Zhu, T., Sharma, P., Watkinson, P.J., Clifton, D.A.: Deep interpretable early warning system for the detection of clinical deterioration. *IEEE Journal of Biomedical and Health Informatics* **24**(2), 437–446 (2020) <https://doi.org/10.1109/JBHI.2019.2937803>
- [4] Wells, B.J., Chagin, K.M., Nowacki, A.S., Kattan, M.W.: Strategies for handling missing data in electronic health record derived data. *Egems* **1**(3) (2013)
- [5] Hu, Z., al.: Strategies for handling missing clinical data for automated surgical site infection detection from the electronic health record. *Journal of biomedical informatics* **68**, 112–120 (2017)
- [6] Mazurowski, M., al.: Training neural network classifiers for medical decision making: The effects of imbalanced datasets on classification performance. *Neural networks* **21**(2-3), 427–436 (2008)
- [7] Wu, J., He, J., Liu, Y.: Imverde: Vertex-diminished random walk for learning imbalanced network representation. In: 2018 IEEE International Conference on Big Data (Big Data), pp. 871–880 (2018). IEEE
- [8] al., R.H.: Relationship between blood pressure and incident chronic kidney disease in hypertensive patients. *Clinical Journal of the American Society of Nephrologists* **6**(11) (2011)
- [9] Yadav, P., Steinbach, M., Kumar, V., Simon, G.: Mining electronic health records (ehrs) a survey. *ACM Computing Surveys (CSUR)* **50**(6), 1–40 (2018)
- [10] Jensen, P.B., Jensen, L.J., Brunak, S.: Mining electronic health records: towards better research applications and clinical care. *Nature Reviews Genetics* **13**(6), 395–405 (2012)
- [11] al., T.E.: A survey on missing data in machine learning. *Journal of Big Data* **8**, 140 (2021)

- [12] Gu, J., Wang, Z., Kuen, J., Ma, L., Shahroudy, A., Shuai, B., Liu, T., Wang, X., Wang, G., Cai, J., *et al.*: Recent advances in convolutional neural networks. *Pattern recognition* **77**, 354–377 (2018)
- [13] Schuster, M., Paliwal, K.K.: Bidirectional recurrent neural networks. *IEEE transactions on Signal Processing* **45**(11), 2673–2681 (1997)
- [14] Arber, S., Hunter, J.J., Ross Jr, J., Hongo, M., Sansig, G., Borg, J., Perriard, J.-C., Chien, K.R., Caroni, P.: Mlp-deficient mice exhibit a disruption of cardiac cytoarchitectural organization, dilated cardiomyopathy, and heart failure. *Cell* **88**(3), 393–403 (1997)
- [15] Sauer, C.M., Chen, L.-C., Hyland, S.L., Girbes, A., Elbers, P., Celi, L.A.: Leveraging electronic health records for data science: common pitfalls and how to avoid them. *The Lancet Digital Health* **4**(12), 893–898 (2022)
- [16] Cao, W., Wang, D., Li, J., Zhou, H., Li, L., Li, Y.: Brits: Bidirectional recurrent imputation for time series. *Advances in neural information processing systems* **31** (2018)
- [17] Che, Z., Purushotham, S., Cho, K., Sontag, D., Liu, Y.: Recurrent neural networks for multivariate time series with missing values. *Scientific reports* **8**(1), 1–12 (2018)
- [18] Yoon, J., Zame, W.R., Schaar, M.: Multi-directional recurrent neural networks: A novel method for estimating missing data. In: *Time Series Workshop in International Conference on Machine Learning* (2017)
- [19] Jun, E., Mulyadi, A.W., Choi, J., Suk, H.-I.: Uncertainty-gated stochastic sequential model for ehr mortality prediction. *IEEE Transactions on Neural Networks and Learning Systems* **32**(9), 4052–4062 (2020)
- [20] Mulyadi, A.W., Jun, E., Suk, H.-I.: Uncertainty-aware variational-recurrent imputation network for clinical time series. *IEEE Transactions on Cybernetics* (2021)
- [21] Luo, Y., Cai, X., Zhang, Y., Xu, J., *et al.*: Multivariate time series imputation with generative adversarial networks. *Advances in neural information processing systems* **31** (2018)
- [22] Mescheder, L., Geiger, A., Nowozin, S.: Which training methods for gans do actually converge? In: *International Conference on Machine Learning*, pp. 3481–3490 (2018). PMLR
- [23] Tashiro, Y., Song, J., Song, Y., Ermon, S.: Csd: Conditional score-based diffusion models for probabilistic time series imputation. *Advances in Neural Information Processing Systems* **34**, 24804–24816 (2021)

- [24] Wen, Q., Zhou, T., Zhang, C., Chen, W., Ma, Z., Yan, J., Sun, L.: Transformers in time series: A survey. arXiv preprint arXiv:2202.07125 (2022)
- [25] Du, W., Côté, D., Liu, Y.: Saits: Self-attention-based imputation for time series. *Expert Systems with Applications* **219**, 119619 (2023)
- [26] Shan, S., Li, Y., Oliva, J.B.: Nrtsi: Non-recurrent time series imputation. In: ICASSP 2023 - 2023 IEEE International Conference on Acoustics, Speech and Signal Processing (ICASSP), pp. 1–5 (2023). <https://doi.org/10.1109/ICASSP49357.2023.10095054>
- [27] Choi, T.-M., Kang, J.-S., Kim, J.-H.: Rdis: Random drop imputation with self-training for incomplete time series data. *IEEE Access* (2023)
- [28] Qian, L., Ibrahim, Z.M., Zhang, A., Dobson, R.J.B.: Addressing class imbalance in electronic health records data imputation. In: Ibrahim, Z.M., Wu, H., Wiratunga, N. (eds.) *Proceedings of the 6th International Workshop on Knowledge Discovery from Healthcare Data Co-located with 32nd International Joint Conference on Artificial Intelligence (IJCAI 2023)*, Macao, China, August 20, 2023. CEUR Workshop Proceedings, vol. 3479. CEUR-WS.org, ??? (2023). <https://ceur-ws.org/Vol-3479/paper7.pdf>
- [29] Pollard, T.J., Johnson, A.E., Raffa, J.D., Celi, L.A., Mark, R.G., Badawi, O.: The eicu collaborative research database, a freely available multi-center database for critical care research. *Scientific data* **5**(1), 1–13 (2018)
- [30] Johnson, A., al.: MIMIC-III, a freely accessible critical care database. *Scientific data* **3**(1), 1–9 (2016)
- [31] Purushotham, S., Meng, C., Che, Z., Liu, Y.: Benchmarking deep learning models on large healthcare datasets. *Journal of biomedical informatics* **83**, 112–134 (2018)
- [32] Harutyunyan, H., Khachatryan, H., Kale, D.C., Ver Steeg, G., Galstyan, A.: Multitask learning and benchmarking with clinical time series data. *Scientific data* **6**(1), 96 (2019)
- [33] Silva, I., Moody, G., Scott, D., Celi, L., Mark, R.: Predicting in-hospital mortality of ICU patients: The physionet/computing in cardiology challenge 2012. *Computational Cardiology* **39**, 245–248 (2012)